ACS APPLIED MATERIALS & INTERFACES

www.acsami.org

Research Article

Implanting Polypyrrole in Metal-Porphyrin MOFs: Enhanced Electrocatalytic Performance for CO_2RR

Zhifeng Xin,* Jingjing Liu, Xinjian Wang, Kejing Shen, Zibo Yuan, Yifa Chen,* and Ya-Qian Lan

Cite This: *ACS Appl. Mater. Interfaces* 2021, 13, 54959−54966

Read Online

ACCESS | Metrics & More | Article Recommendations | Supporting Information

ABSTRACT: Metal−organic frameworks (MOFs) with plenty of active sites and high porosity have been considered as an excellent platform for the electroreduction of CO_2, yet they are still restricted by the low conductivity or low efficiency. Herein, we insert the electron-conductive polypyrrole (PPy) molecule into the channel of MOFs through the in situ polymerization of pyrrole in the pore of MOF-545-Co to increase the electron-transfer ability of MOF-545-Co and the obtained hybrid materials present excellent electrocatalytic CO_2RR performance. For example, FE_{CO} of PPy@MOF-545-Co can reach up to 98% at −0.8 V, almost 2 times higher than that of bare MOF-545-Co. The high performance might be attributed to the incorporation of PPy that can serve as electric cables in the channel of MOF to facilitate electron transfer during the CO_2RR process. This attempt might provide new insights to improve the electrocatalytic performance of MOFs for CO_2RR.

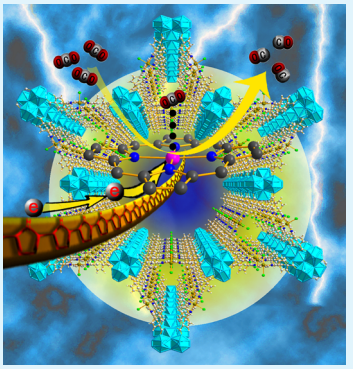

KEYWORDS: *polypyrrole, metalloporphyrin organic framework, electrocatalytic performance, electron transfer, CO_2RR*

INTRODUCTION

The increasing emission amount of carbon dioxide (CO_2) has led to severe environmental issues and even irreversible climate changes such as sea level rising or land desertification, and so forth.[1] Under this circumstance, converting CO_2 into fuels or other high-valued chemicals is considered as one of the most important ways to address this threat.[2,3] Various techniques for storing or transforming CO_2 have been studied,[4] during which, the electrocatalytic CO_2 reduction reaction (CO_2RR) as a sort of high-efficiency and controllable method has been deemed as one of the most promising approaches to convert CO_2 into energy products (e.g., CO, HCOOH, C_2H_5OH, and CH_4).[5−10] Over the past years, numerous researchers devote themselves to the development of highly active electrocatalytic materials for CO_2RR[11−15] and various materials including metals,[16,17] transition-metal chalcogenides,[18] transition-metal oxides,[19] metal-free two-dimensional materials,[20−22] and MOFs[23−28] have been investigated. Several primary principles for the design of CO_2RR electrocatalysts should be considered: (1) highly active catalytic sites; (2) sufficient surface area; and (3) efficient electron-transfer ability. While many interesting materials have been studied, the low selectivity or instability of the materials has largely hindered the progress of electrocatalytic CO_2RR to a great extent.

Among various alternatives, the controllable active metal sites and organic ligands of MOFs make it an ideal electrocatalytic platform for electrocatalytic CO_2RR. The high porosity and plenty of metal sites endow MOFs with favorable capability for establishing desired catalytic environments for CO_2RR.[29−36] However, the low electron transfer and donating ability have largely restricted most of MOFs in the efficient electrocatalytic CO_2RR, especially for the multiple electron-transfer necessity during the reduction processes. Thus, increasing the charge-transfer ability of catalytic sites in MOFs might enhance the electrocatalytic activity and selectivity for CO_2RR. To address these issues, various methods have been carried out, such as introducing ligands or metal clusters with high electron density, adding electron-rich molecules into MOF structures,[37−39] and so forth. However, the difficulty in material design or complicated processes have restricted their wide-spread applications and feasible strategies that enable facile processing of MOFs into valuable CO_2RR electrocatalysts are much desired yet largely unmet.[40−43]

With these considerations in mind, polypyrrole (PPy), as a kind of powerful conductive polymer, comes to our mind as a desired additive to be hybridized with MOFs to achieve efficient CO_2RR systems. We intend to assemble PPy in the channel of MOF-545-Co for the following reasons: (1) PPy is one of the extensively investigated conductive polymers due to its potential applications in various devices and has been proposed that the introduction of PPy into the structure of

Received: August 10, 2021
Accepted: November 2, 2021
Published: November 12, 2021

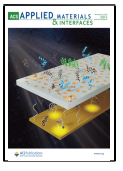

MOFs will largely improve the electron-transfer ability;[44,45] (2) MOF-545-Co possess high porosity, uniformly distributed active sites, and large pore size that can provide enough space for PPy loading and CO_2RR; and (3) the synergistic integration of them might create a powerful catalysis system that can endow high electron-transfer ability to MOFs for efficient CO_2RR. As far as we know, this kind of catalytic system has been rarely reported.

Herein, a feasible in situ low-temperature polymerization method has been reported to synthesize a series of PPy@MOF-545-M (M = Fe, Co, and Ni) hybrid materials and successfully apply them in electrocatalytic CO_2RR. In the obtained PPy@MOF-545-Co, the PPy molecule is similar to a cable in the MOF channel, which can transfer electrons to the active center of Co-TCPP more smoothly and greatly improve the electrocatalytic activity for CO_2RR (Figure 1). Specifically,

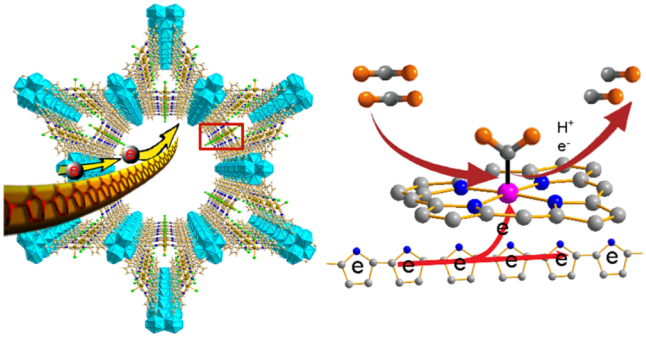

Figure 1. Schematic presentation for the advantages of PPy in the channel of MOF-545-Co for electrocatalytic CO_2RR.

PPy@MOF-545-Co can convert CO_2 to CO with a high selectivity (98%, −0.8 V), almost 2 times higher than that of MOF-545-Co. Besides, the catalyst can be durable for 10 h with remained crystallinity and property.

RESULTS AND DISCUSSION

Zr_6O_8 clusters assembled with Co-TCPP generated two kinds of pores (16 and 36 Å) in the structure of MOF-545-Co, which can supply enough space to encapsulate PPy molecules (diameter about 4.5 Å). Powder X-ray diffraction (PXRD) patterns demonstrate that the framework still maintains the structure of MOF-545-Co after the loading of PPy (Figure 1a). However, the PPy peaks were hardly observed in the PXRD pattern of PPy@MOF-545-Co due to both the small size of PPy molecules and their extremely low amount when compared with the host MOF.[46] The morphology of PPy@MOF-545-Co was investigated by scanning electron microscopy (SEM) and transition electron microscopy (TEM). As shown in Figures 2c,d and Figure S1, the as-prepared PPy@MOF-545-Co displays rod-like shape with a diameter of ∼100 nm and a length of ∼500 nm. Specifically, the morphology of MOF-545-Co remained unchanged during the loading process of PPy.[37] The PPy-loaded PPy@MOF-545-Co rod shows a smooth surface, which indicates that PPy polymerizes into the pore channel of MOF without the residues on the surface. Moreover, the elements of Co, Zr, C, and N are evenly dispersed in the rod-like particles of PPy@MOF-545-Co as shown in the energy-dispersive X-ray spectroscopy (EDS) elemental mapping images (Figure 2e). To investigate the catalytic performance of PPy in MOF with different metals, the PPy molecule was also introduced into both MOF-545-Fe and MOF-545-Ni through the similar procedures as that of PPy@MOF-545-Co. The PXRD patterns (Figure S2a) show that PPy@MOF-545-Fe and PPy@MOF-545-Ni can maintain the structure of MOF-545.

The encapsulation of PPy in MOF-545-Co was also proved by the IR spectrum, which displayed the characteristic peaks of PPy (Figure S3). The peaks at 1555 and 964 cm^{-1} were ascribed to the stretching vibration of Py rings and PPy, respectively. Besides, the peaks at 1053 and 1306 cm^{-1} corresponded to the C−H deformation vibrations and C−N stretching vibrations, respectively.[12,40] In addition, the N_2 sorption isotherms of PPy@MOF-545-Co and the contrast samples (i.e. MOF-545 and MOF-545-Co) were obtained to study the porosity and surface areas of the obtained materials. The Brunauer−Emmett−Teller surface areas (S_{BET}) of MOF-545, MOF-545-Co, and PPy @MOF-545-Co were calculated to be 1958, 1716, and 146.6 m^2/g, respectively (Figure 2b and Table S1). This obvious decrease of S_{BET} and pore volume (Figure S4) resulted from the encapsulation of PPy in the pore of MOF-545-Co. The high-resolution TEM image showed the observed crystalline lattice structure of PPy@MOF-545-Co (Figure S5). When the PPy molecule formed in the MOF channels, the host−guest $\pi-\pi$ interaction between the PPy molecule and TCPP ligand in MOF might be beneficial for the charge transfer.[46] To further study the effect of PPy on the performance, we introduced different amounts of PPy in MOF-545-Co and tested the catalytic performance for CO_2RR. The PPy@MOF-545-Co with different PPy loadings was also prepared and characterized by PXRD and N_2 sorption measurement. The PXRD patterns showed that the structure of MOF-545-Co was still maintained after the loading of different amounts of PPy (Figure S6a). The N_2 sorption measurement showed that S_{BET} increased with the decrease of the PPy loading amount in the MOF channel (Figure S6b and Table S1), which implies that the different loading amount of PPy would partially occupy different pore volume of MOF.

To further support the high porosity, CO_2 adsorption measurements were also performed. From the results of CO_2 uptake curves, the CO_2 capacities of MOF-545, MOF-545-Co, and PPy@MOF-545-Co were tested to be 39, 48, and 12 cm^3/g at 298 K, respectively (Figure S7a). The difference of CO^2 uptake results from the loading of PPy, which affects the porosity of MOFs. In addition, the adsorption enthalpy of PPy@MOF-545-Co, MOF-545-Co, and MOF-545 (Figure S7b) were calculated based on the CO_2 adsorption curves obtained at 273, 283, and 298 K. The CO_2 adsorption enthalpy of PPy@MOF-545-Co (44 kJ/mol) was higher than that of MOF-545-Co (34.5 kJ/mol) and MOF-545 (19.5 kJ/mol). The results indicated that the introduction of PPy was favorable for the adsorption of CO_2.

Thermogravimetric analysis (TGA) was also used to test the loading amount of Py in the channels of MOF-545-Co. In the TGA curve of Py@MOF-545-Co, the initial weight loss of 17% from 25 to 200 °C belongs to the loss of Py in the channel, which indicates that the loading of Py is about 17% (Figure S9), which was in accordance with the amount of isolated PPy from PPy@MOF-545-Co.[39,47] This result also indicated that all the adsorbed Py polymerized into PPy in the channel of MOF-545-Co.

The electrocatalytic CO_2RR tests were conducted in an electrochemical H-type cell. The electrochemical properties of PPy@MOF-545-Co, MOF-545-Co, PPy@MOF-545, and PPy were studied using a three-electrode system in 0.5 M $KHCO_3$

https://doi.org/10.1021/acsami.1c15187
ACS Appl. Mater. Interfaces 2021, 13, 54959−54966

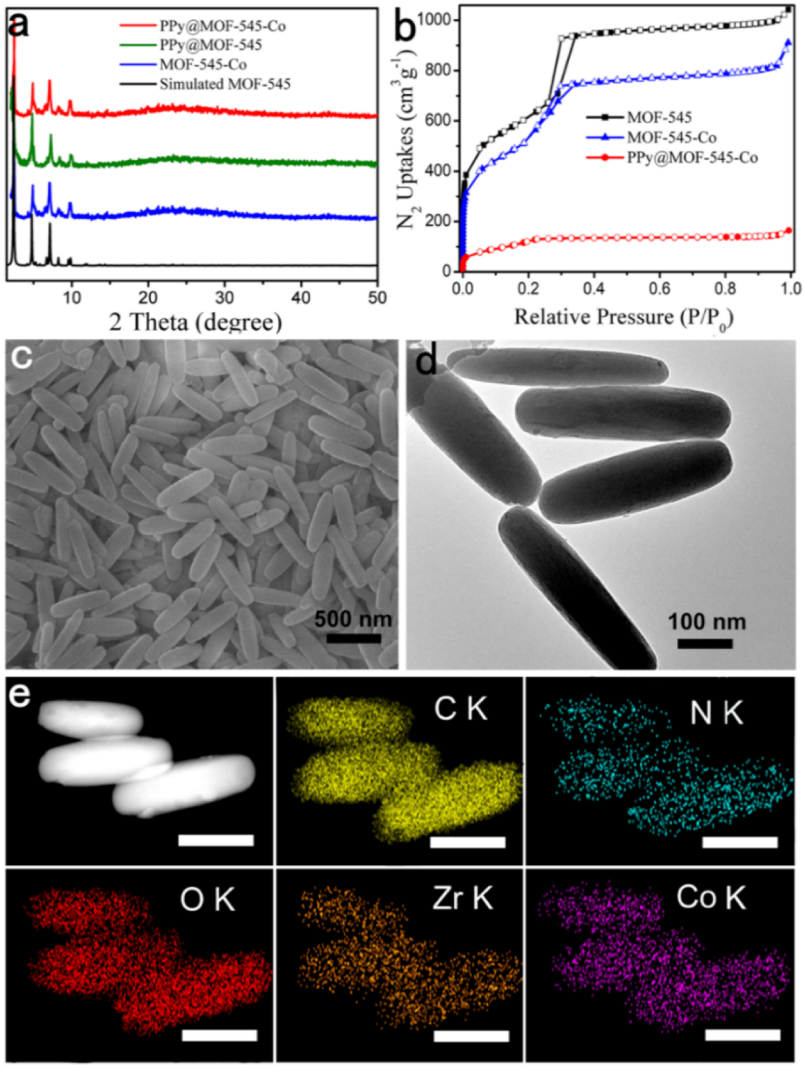

Figure 2. Characterization of PPy@MOF-545-Co. (a) PXRD patterns of PPy@MOF-545-Co, MOF-545-Co, MOF-545, and simulated MOF-545. (b) N_2 sorption isotherms of PPy@MOF-545-Co, MOF-545-Co, and MOF-545 measured at 77 K. (c) SEM image of PPy@MOF-545-Co. (d) TEM image of PPy@MOF-545-Co. (e) Scanning TEM-high-angle annular dark field image and EDS elemental mapping of MOF-545-Co (scale bar is 200 nm).

solution. The linear sweep voltammetry (LSV) curves showed the variation trend of current with the increase of voltage. The current of PPy@MOF-545-Co in the LSV curve increased sharply after −0.42 V, and the largest current density was 32 mA cm^{-2} at −1.1 V, which was largely higher than that of MOF-545-Co, PPy@MOF-545, and PPy (Figure 3a). The higher current density of PPy@MOF-545-Co indicated the higher electrocatalysis activity for CO_2 reduction compared with MOF-545-Co, PPy@MOF-545, and PPy. To further detect the electrochemical performance of PPy@MOF-545-Co, the LSV curves were tested in both CO_2-saturated and Ar-saturated $KHCO_3$ solution (Figure 3b). The higher current density measured under CO_2-saturated $KHCO_3$ solution than that under Ar-saturated $KHCO_3$ solution indicated that the current increasing mainly came from CO_2RR (Figure 3b).[48] The gaseous and liquid products were detected by gas chromatography (GC) and ^{1}H nuclear magnetic resonance spectroscopy, respectively (Figure S11). The result exhibited that no liquid product was detected and CO was the main gas product.[49] Moreover, the FEs and current density tests were conducted to study the performances of samples (i.e., PPy@MOF-545-Co, MOF-545-Co, PPy, and PPy@MOF-545). The FE_{CO} of PPy@MOF-545-Co increased with the increase of potential and reached the peak (98%) at −0.8 V, and the overall FE_{CO} level kept well above 75% under the potentials ranging from −0.5 to −1.0 V [vs reversible hydrogen electrode (RHE)]. The maximum FE_{CO} value (Figure 3c) of PPy@MOF-545-Co was 98% at −0.8 V, which was remarkably higher than that of MOF-545-Co (57%, −0.8 V), PPy (12%, −0.7 V), and Py@MOF-545 (26%, −0.6 V). The higher CO partial current density of PPy@MOF-545-Co (13 mA cm^{-2} at −1.0 V) than contrast samples indicated the better electron-transfer ability in the CO_2RR process (Figure 3d). Noteworthy, the FE_{CO} value (98%, −0.8 V) was also higher than most of the metalloporphyrin MOFs (Figure 3e).[23,24,33,34] To select the most suitable active metal site in the MOF structure, we selected MOF-545-Co, MOF-545-Ni, and MOF-545-Fe to load PPy and further test their catalytic performances. The result indicated that PPy@MOF-545-Co showed a higher FE_{CO} value than PPy@MOF-545-Fe (89.2%, −0.7 V) and PPy@MOF-545-Ni (87.8%, −0.9 V) (Figure S1b). Therefore,

https://doi.org/10.1021/acsami.1c15187
ACS Appl. Mater. Interfaces 2021, 13, 54959−54966

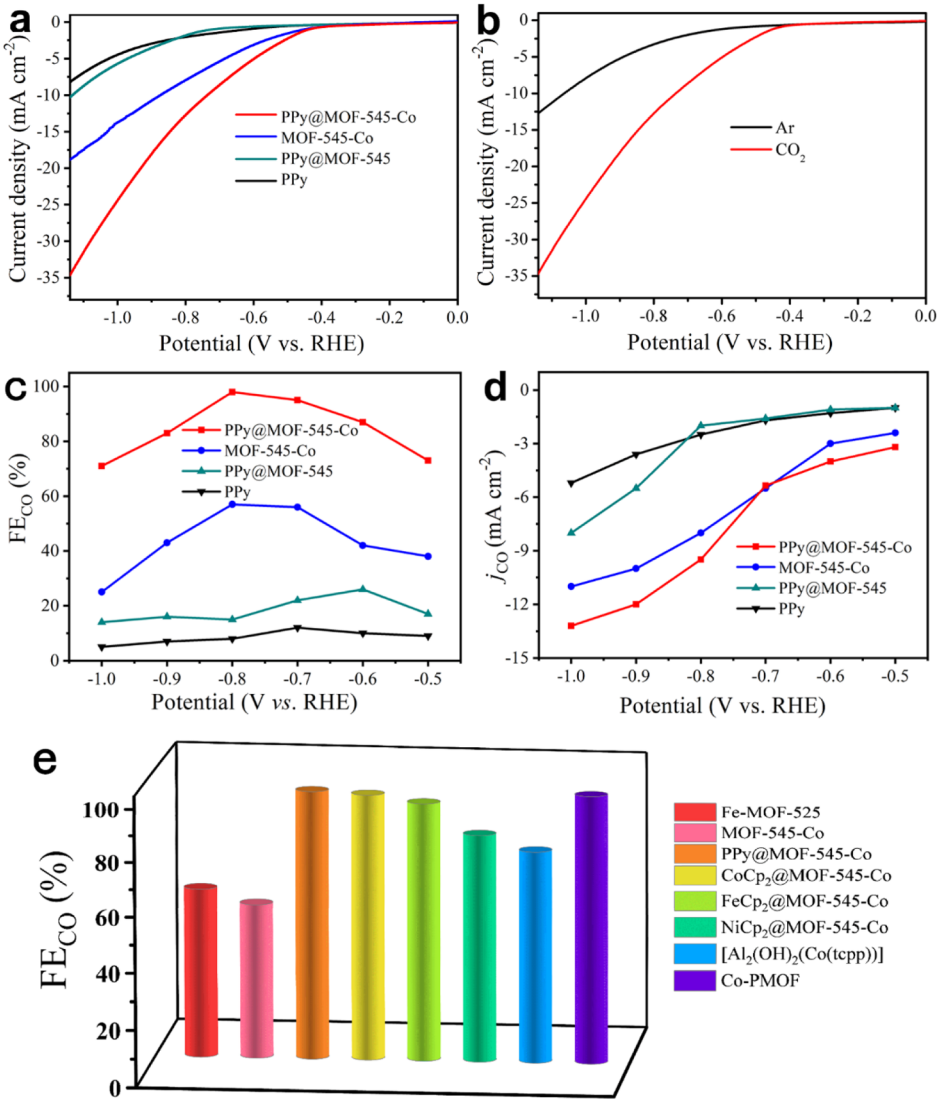

Figure 3. Electrocatalytic CO_2RR performance of PPy@MOF-545-Co. (a) LSV curves of PPy@MOF-545-Co and contrastive samples. (b) LSV curves of PPy@MOF-545-Co at CO_2- and Ar-saturated 0.1 M $KHCO_3$. (c) FE_{CO} of PPy@MOF-545-Co and contrastive samples measured under different voltages. (d) Partial CO current density. (e) Summary of electrocatalytic performances of the literature-reported materials and metal-doped porphyrin MOFs.

we choose PPy-loaded MOF-545-Co as a desired platform for further investigation.

To further investigate the specific catalytic performance of PPy@MOF-545-Co, a series of comparison samples [i.e., MOF-545, MOF-545-Co, PPy, and physical mixture (MOF-545-Co/PPy with a ratio of 83/17)] were prepared to test their performances (Figure S12). For these samples, MOF-545-Co (FE_{CO} = 57%, −0.8 V) and MOF-545-Co/PPy (62%, −0.8 V) exhibited lower catalytic performance than PPy@MOF-545-Co (98%, −0.8 V), which could be ascribed to the lower electron-transfer ability. On the contrary, MOF-545 and PPy exhibited a negligible catalytic activity for CO_2 reduction, which might be explained by the absence of Co active sites that resulted in a sharp decrease of catalytic activity. It also implies that the notable electrocatalytic performance of PPy@MOF-545-Co origins from the cooperation effect between Co-TCPP and PPy molecules. To further study the effect of PPy on the catalytic performance of MOF, we tested the CO_2RR catalytic performance of PPy@MOF-545-Co with different amounts of PPy. To investigate the effect of PPy, we applied three diverse loading amounts of PPy in MOF-54-Co to test the catalytic performance. We obtained the hybrid MOF materials with pure Py (denoted as PPy@MOF-545-Co), half the amount of Py [denoted as PPy@MOF-545-Co (1/2)], and quarter the amount of Py [denoted as PPy@MOF-545-Co (1/4)], respectively. Figure 4e shows the FE_{CO} for MOF with different Py loadings, and the result indicated that the catalytic performance increased with the enhancement of Py loading. This might be because pure Py loaded in MOF channels can polymerize into continuous PPy molecules. When the concentration of Py decreased, the shorter PPy chain might be formed. Under these circumstances, it is difficult to form a continuous electron transport medium, thus resulting in lower catalytic performance. As seen in Figure 4e, when the PPy loading amount decreases, FE_{CO} gradually decreases from 98 (PPy@MOF-545-Co) to 87% [PPy@MOF-545-Co (1/4)]. In addition, the calculated turnover frequency (TOF) of PPy@MOF-545-Co was up to about 785 h^{-1} at a potential of −1.0 V (vs hydrogen evolution reaction), which is superior to that of MOF-545-Co and other contrast samples (Figure 4b).

https://doi.org/10.1021/acsami.1c15187
ACS Appl. Mater. Interfaces 2021, 13, 54959−54966

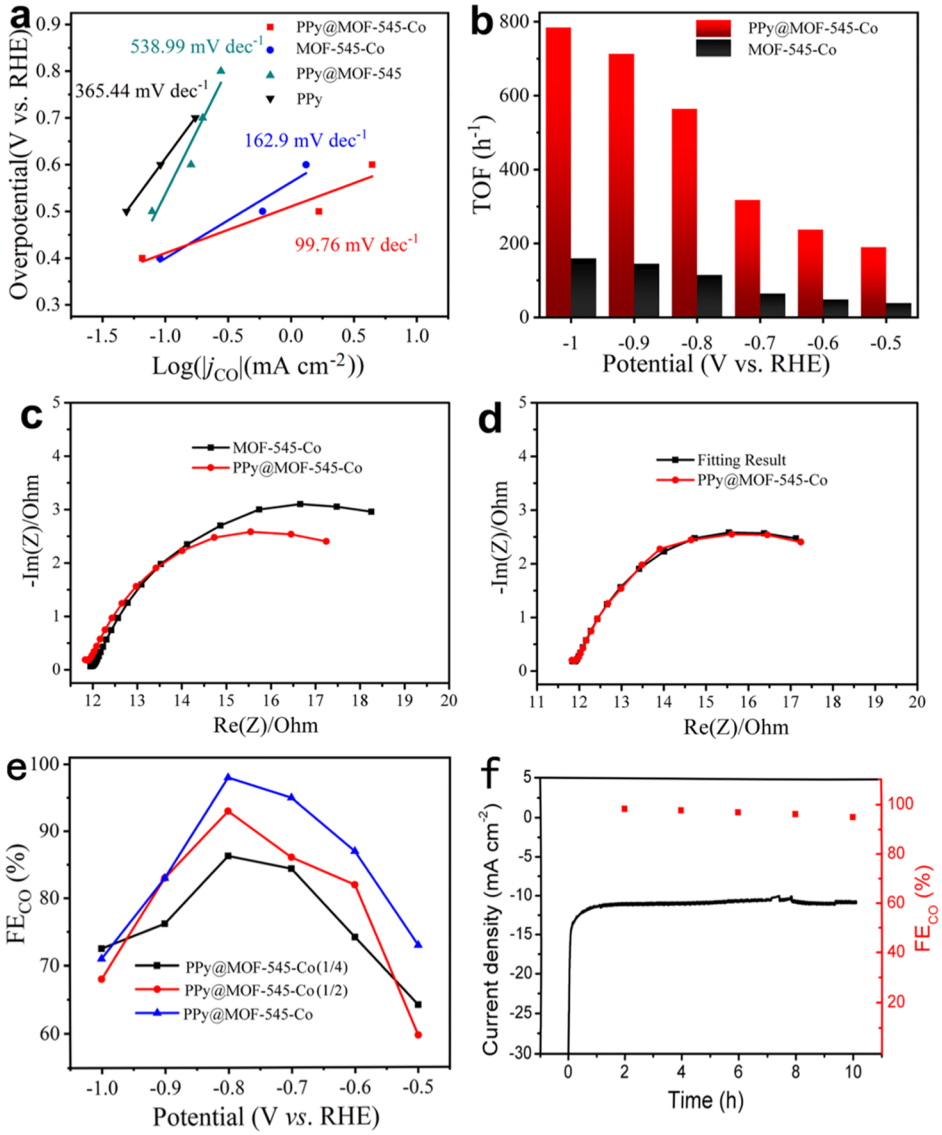

Figure 4. Electrocatalytic CO_2RR performances of PPy@MOF-545-Co and contrast samples. (a) Tafel plots of PPy@MOF-545-Co and contrastive samples. (b) TOF of PPy@MOF-545-Co and MOF-545-Co at different potentials. (c) Nyquist plots of PPy@MOF-545-Co and MOF-545-Co. (d) PPy@MOF-545-Co fitting result over the frequency ranging from 1000 kHz to 0.1 Hz at −0.8 V vs RHE. (e) FE_{CO} of PPy@MOF-545-Co, PPy@MOF-545-Co (1/2), and PPy@MOF-545-Co (1/4) at different potentials. (f) Durability test of PPy@MOF-545-Co at a potential of −0.8 V vs RHE.

To evaluate the electrocatalysis stability, the durability of CO_2RR has been measured. The current density of PPy@MOF-545-Co remained almost constant (about −11 mA cm^{-1}), and FE_{CO} maintained 95% of the initial FE for CO production after 10 h of continuous electrolysis at −0.8 V (Figure 4f). Besides, the PXRD pattern indicated that the structure remained unchanged after 10 h of the electrocatalytic reaction, which implied high stability during the electrocatalytic reaction (Figure S13).

Tafel slope was an important parameter often used to characterize the performance of an electrochemical catalyst as it quantified the amount of additional applied potential required to observe the logarithmic increase in the measured current.[50] The smaller the slope of the Tafel curve, the lower the overpotential of the catalytic process under the same kinetic current density or apparent current density. The Tafel slopes of PPy@MOF-545-Co was 99.8 (mV dec^{-1}), which was obviously smaller than those of MOF-545-Co (162.9 mV dec^{-1}), PPy@MOF-545 (539.0 mV dec^{-1}), and PPy (365.4 mV dec^{-1}), suggesting that PPy@MOF-545-Co has the most favorable kinetics for the reduction of CO_2 and excellent catalytic activity (Figure 4a). Electrochemical impedance spectroscopy was generally applied to analyze the structure of the electrochemical system and the properties of the electrode process. As shown in the Nyquist plots (Figure 4c), the charge-transfer resistance (R_{ct}) of PPy@MOF-545-Co was 7.5 Ω, which was lower than that of MOF-545-Co (12.5 Ω), demonstrating that PPy@MOF-545-Co possessed much lower charge-transfer resistance in the electron-transfer process. The electron conductivity test further proved that the loading of PPy enhanced the electron conductivity of MOF-545-Co to a certain extent (Figure S9). This would be attributed to the possible interactions (e.g., $\pi-\pi$ interaction or van der Waals force) between PPy molecules and Co-TCPP center of MOF-545-Co might enhance the charge-transfer ability for the active site in the CO_2RR process.

https://doi.org/10.1021/acsami.1c15187
ACS Appl. Mater. Interfaces 2021, 13, 54959−54966

CONCLUSIONS

In summary, a feasible low-temperature in situ polymerization method has been applied to impart oriented PPy chains in the pores of MOF-545-Co. This method not only preserves the catalytic sites in the host framework but also improves the electrochemical conductivity of the materials, which is much beneficial for the improvement of CO_2RR performance. Specifically, the FE_{CO} of PPy@MOF-545-Co reaches as high as 98% at −0.8 V, almost 2 times higher than that of bare MOF-545-Co. The high performance might be attributed to the incorporation of PPy that can serve as electric cables in the channel of MOF that facilitate electron transfer during the CO_2RR process. This method will pave a promising pathway for the design of high-efficiency catalysts and should inject new vitality not only to CO_2 reduction research but also to the extensive electrocatalytic field.

ASSOCIATED CONTENT

Supporting Information

The Supporting Information is available free of charge at https://pubs.acs.org/doi/10.1021/acsami.1c15187.

Details of synthesis; material characterizations; XRD patterns; additional SEM, TEM images; XPS spectra; and electrochemical characterizations (PDF)

AUTHOR INFORMATION

Corresponding Authors

Zhifeng Xin − *Institute of Molecular Engineering and Applied Chemistry, Anhui University of Technology, Ma'anshan, Anhui 243002, P. R. China;* orcid.org/0000-0001-9080-9695; Email: xinzf521@ahut.edu.cn

Yifa Chen − *Jiangsu Collaborative Innovation Centre of Biomedical Functional Materials, Jiangsu Key Laboratory of New Power Batteries, School of Chemistry and Materials Science, Nanjing Normal University, Nanjing 210023, P. R. China;* orcid.org/0000-0002-1718-6871; Email: chyf927821@163.com

Authors

Jingjing Liu − *Institute of Molecular Engineering and Applied Chemistry, Anhui University of Technology, Ma'anshan, Anhui 243002, P. R. China*

Xinjian Wang − *Institute of Molecular Engineering and Applied Chemistry, Anhui University of Technology, Ma'anshan, Anhui 243002, P. R. China*

Kejing Shen − *Institute of Molecular Engineering and Applied Chemistry, Anhui University of Technology, Ma'anshan, Anhui 243002, P. R. China*

Zibo Yuan − *Institute of Molecular Engineering and Applied Chemistry, Anhui University of Technology, Ma'anshan, Anhui 243002, P. R. China*

Ya-Qian Lan − *Jiangsu Collaborative Innovation Centre of Biomedical Functional Materials, Jiangsu Key Laboratory of New Power Batteries, School of Chemistry and Materials Science, Nanjing Normal University, Nanjing 210023, P. R. China;* orcid.org/0000-0002-2140-7980

Complete contact information is available at: https://pubs.acs.org/10.1021/acsami.1c15187

Author Contributions

Z.X., Y.C., and Y.-Q.L instructed this work and cowrote this paper. J.L., X.W., and Z.Y. carried out the experiments. K.S. contributed to the GC spectrum measurement.

Notes

The authors declare no competing financial interest.

ACKNOWLEDGMENTS

This work was financially supported by the National Natural Science Foundation of China (nos. 22171139, 21471003, 21871141, 21871142, 21701085, and 21901122); Natural Science Foundation of Educational Commission of Anhui Province of China (no. KJ2020A0240); the Natural Science Research of Jiangsu Higher Education Institutions of China (no. 19KJB150011); and Project funded by China Postdoctoral Science Foundation (no. 2019M651873).

REFERENCES

(1) Shakun, J. D.; Clark, P. U.; He, F.; Marcott, S. A.; Mix, A. C.; Liu, Z.; Otto-Bliesner, B.; Schmittner, A.; Bard, E. Global Warming Preceded by Increasing Carbon Dioxide Concentrations During the Last Deglaciation. *Nature* **2012**, *484*, 49−54.

(2) Dowell, N. M.; Fennell, P. S.; Shah, N.; Maitland, G. C. The Role of CO_2 Capture and Utilization in Mitigating Climate Change. *Nat. Clim. Change* **2017**, *7*, 243−249.

(3) Qiao, J.; Liu, Y.; Hong, F.; Zhang, J. A Review of Catalysts for the Electroreduction of Carbon Dioxide to Produce Low-Carbon Fuels. *Chem. Soc. Rev.* **2014**, *43*, 631−675.

(4) Sumida, K.; Rogow, D. L.; Mason, J. A.; McDonald, T. M.; Bloch, E. D.; Herm, Z. R.; Bae, T.-H.; Long, J. R. Carbon Dioxide Capture in Metal-Organic Frameworks. *Chem. Rev.* **2012**, *112*, 724−781.

(5) Liao, P.-Q.; Shen, J.-Q.; Zhang, J.-P. Metal-Organic Frameworks for Electrocatalysis. *Coord. Chem. Rev.* **2018**, *373*, 22−48.

(6) Pan, Y.; Lin, R.; Chen, Y.; Liu, S.; Zhu, W.; Cao, X.; Chen, W.; Wu, K.; Cheong, W.-C.; Wang, Y.; Zheng, L.; Luo, J.; Lin, Y.; Liu, Y.; Liu, C.; Li, J.; Lu, Q.; Chen, X.; Wang, D.; Peng, Q.; Chen, C.; Li, Y. Design of Single-Atom Co−N_5 Catalytic Site: A Robust Electrocatalyst for CO_2 Reduction with Nearly 100% CO Selectivity and Remarkable Stability. *J. Am. Chem. Soc.* **2018**, *140*, 4218−4221.

(7) Jiao, J.; Lin, R.; Liu, S.; Cheong, W.-C.; Zhang, C.; Chen, Z.; Pan, Y.; Tang, J.; Wu, K.; Hung, S.-F.; Chen, H. M.; Zheng, L.; Lu, Q.; Yang, X.; Xu, B.; Xiao, H.; Li, J.; Wang, D.; Peng, Q.; Chen, C.; Li, Y. Copper Atom-Pair Catalyst Anchored on Alloy Nanowires for Selective and Efficient Electrochemical Reduction of CO_2. *Nat. Chem.* **2019**, *11*, 222−228.

(8) Rao, H.; Schmidt, L. C.; Bonin, J.; Robert, M. Visible-Light-Driven Methane Formation from CO_2 With a Molecular Iron Catalyst. *Nature* **2017**, *548*, 74−77.

(9) De Luna, P.; Quintero-Bermudez, R.; Dinh, C.-T.; Ross, M. B.; Bushuyev, O. S.; Todorović, P.; Regier, T.; Kelley, S. O.; Yang, P.; Sargent, E. H. Catalyst Electro-Redeposition Controls Morphology and Oxidation State for Selective Carbon Dioxide Reduction. *Nat. Catal.* **2018**, *1*, 103−110.

(10) Yi, J. D.; Xie, R.; Xie, Z. L.; Chai, G. L.; Liu, T. F.; Chen, R. P.; Huang, Y. B.; Cao, R. Highly Selective CO_2 Electroreduction to CH_4 by In Situ Generated Cu_2O Single-Type Sites on a Conductive MOF: Stabilizing Key Intermediates with Hydrogen Bonding. *Angew. Chem., Int. Ed.* **2020**, *59*, 23641−23648.

(11) Chen, C.; Yan, X.; Liu, S.; Wu, Y.; Wan, Q.; Sun, X.; Zhu, Q.; Liu, H.; Ma, J.; Zheng, L.; Wu, H.; Han, B. Highly Efficient Electroreduction of CO_2 to C^{2+} Alcohols on Heterogeneous Dual Active Sites. *Angew. Chem., Int. Ed.* **2020**, *59*, 16459−16464.

(12) Zhang, Y.; Jiao, L.; Yang, W.; Xie, C.; Jiang, H. L. Rational Fabrication of Low-Coordinate Single-Atom Ni Electrocatalysts by MOFs for Highly Selective CO_2 Reduction. *Angew. Chem., Int. Ed.* **2021**, *60*, 7607−7611.

(13) Huang, Q.; Liu, J.; Feng, L.; Wang, Q.; Guan, W.; Dong, L.-Z.; Zhang, L.; Yan, L.-K.; Lan, Y.-Q.; Zhou, H.-C. Multielectron Transportation of Polyoxometalate-Grafted Metalloporphyrin Coordination Frameworks for Selective CO_2-to-CH_4 Photoconversion. *Natl. Sci. Rev.* **2020**, *7*, 53−63.
(14) Lin, R.; Ma, X.; Cheong, W.-C.; Zhang, C.; Zhu, W.; Pei, J.; Zhang, K.; Wang, B.; Liang, S.; Liu, Y.; Zhuang, Z.; Yu, R.; Xiao, H.; Li, J.; Wang, D.; Peng, Q.; Chen, C.; Li, Y. PdAg Bimetallic Electrocatalyst for Highly Selective Reduction of CO_2 with Low COOH* Formation Energy and Facile CO Desorption. *Nano Res.* **2019**, *12*, 2866−2871.
(15) Hou, Y.; Huang, Y.-B.; Liang, Y.-L.; Chai, G.-L.; Yi, J.-D.; Zhang, T.; Zang, K.-T.; Luo, J.; Xu, R.; Lin, H.; Zhang, S.-Y.; Wang, H.-M.; Cao, R. Unraveling the Reactivity and Selectivity of Atomically Isolated Metal−Nitrogen Sites Anchored on Porphyrinic Triazine Frameworks for Electroreduction of CO_2. *CCS Chem.* **2019**, *1*, 384−395.
(16) Li, Q.; Fu, J.; Zhu, W.; Chen, Z.; Shen, B.; Wu, L.; Xi, Z.; Wang, T.; Lu, G.; Zhu, J.-J.; Sun, S. Tuning Sn-Catalysis for Electrochemical Reduction of CO_2 to CO via the Core/Shell Cu/SnO_2 Structure. *J. Am. Chem. Soc.* **2017**, *139*, 4290−4293.
(17) Zhang, W.; Hu, Y.; Ma, L.; Zhu, G.; Wang, Y.; Xue, X.; Chen, R.; Yang, S.; Jin, Z. Progress and Perspective of Electrocatalytic CO_2 Reduction for Renewable Carbonaceous Fuels and Chemicals. *Adv. Sci.* **2018**, *5*, 1700275.
(18) Asadi, M.; Kim, K.; Liu, C.; Addepalli, A. V.; Abbasi, P.; Yasaei, P.; Phillips, P.; Behranginia, A.; Cerrato, J. M.; Haasch, R.; Zapol, P.; Kumar, B.; Klie, R. F.; Abiade, J.; Curtiss, L. A.; Salehi-Khojin, A. Nanostructured Transition Metal Dichalcogenide Electrocatalysts for CO_2 Reduction in Ionic Liquid. *Science* **2016**, *353*, 467−470.
(19) Gao, S.; Lin, Y.; Jiao, X.; Sun, Y.; Luo, Q.; Zhang, W.; Li, D.; Yang, J.; Xie, Y. Partially Oxidized Atomic Cobalt Layers for Carbon Dioxide Electroreduction to Liquid Fuel. *Nature* **2016**, *529*, 68.
(20) Duan, X.; Xu, J.; Wei, Z.; Ma, J.; Guo, S.; Wang, S.; Liu, H.; Dou, S. Metal-Free Carbon Materials for CO_2 Electrochemical Reduction. *Adv. Mater.* **2017**, *29*, 1701784.
(21) Sun, Z.; Ma, T.; Tao, H.; Fan, Q.; Han, B. Fundamentals and Challenges of Electrochemical CO_2 Reduction Using Two-Dimensional Materials. *Chem* **2017**, *3*, 560−587.
(22) Zhao, S.; Wang, D. W.; Amal, R.; Dai, L. Carbon-Based Metal-Free Catalysts for Key Reactions Involved in Energy Conversion and Storage. *Adv. Mater.* **2019**, *31*, 1801526.
(23) Ye, L.; Liu, J.; Gao, Y.; Gong, C.; Addicoat, M.; Heine, T.; Wöll, C.; Sun, L. Highly Oriented MOF Thin Film-Based Electrocatalytic Device for the Reduction of CO_2 to CO Exhibiting High Faradaic Efficiency. *J. Mater. Chem. A* **2016**, *4*, 15320−15326.
(24) Wang, Y.; Hou, P.; Wang, Z.; Kang, P. Zinc Imidazolate Metal−Organic Frameworks (ZIF-8) for Electrochemical Reduction of CO_2 to CO. *ChemPhysChem* **2017**, *18*, 3142−3147.
(25) Rodriguez-Albelo, L. M.; Albelo, R.; Ruiz-Salvador, A. R.; Sampieri, A.; Lewis, D. W.; Gómez, A.; Nohra, B.; Mialane, P.; Marrot, J.; Sécheresse, F.; Mellot-Draznieks, C.; Biboum, R.N.; Keita, B.; Nadjo, L.; Dolbecq, A. Zeolitic Polyoxometalate-Based Metal-organic Frameworks (Z-POMOFs): Computational Evaluation of Hypothetical Polymorphs and the Successful Targeted Synthesis of the Redox-Active ZPOMOF1. *J. Am. Chem. Soc.* **2009**, *131*, 16078−16087.
(26) Hod, I.; Sampson, M. D.; Deria, P.; Kubiak, C. P.; Farha, O. K.; Hupp, J. T. Fe-Porphyrin-Based Metal-Organic Framework Films as High-Surface Concentration, Heterogeneous Catalysts for Electrochemical Reduction of CO_2. *ACS Catal.* **2015**, *5*, 6302−6309.
(27) Kung, C.-W.; Audu, C. O.; Peters, A. W.; Noh, H.; Farha, O. K.; Hupp, J. T.; Hupp, J. T. Copper Nanoparticles Installed in Metal-Organic Framework thin Films are Electrocatalytically Competent for CO_2 Reduction. *ACS Energy Lett.* **2017**, *2*, 2394−2401.
(28) Yi, J. D.; Si, D. H.; Xie, R.; Yin, Q.; Zhang, M. D.; Wu, Q.; Chai, G. L.; Huang, Y. B.; Cao, R. Conductive Two-Dimensional Phthalocyanine-based Metal−Organic Framework Nanosheets for Efficient Electroreduction of CO_2. *Angew. Chem. Int. Ed.* **2021**, *60*, 17108−17114.
(29) Kang, X.; Zhu, Q.; Sun, X.; Hu, J.; Zhang, J.; Liu, Z.; Han, B. Highly Efficient Electrochemical reduction of CO_2 to CH_4 in an Ionic Liquid Using a Metal-Organic Framework Cathode. *Chem. Sci.* **2016**, *7*, 266−273.
(30) Lin, S.; Diercks, C. S.; Zhang, Y.-B.; Kornienko, N.; Nichols, E. M.; Zhao, Y.; Paris, A. R.; Kim, D.; Yang, P.; Yaghi, O. M.; Chang, C. J. Covalent Organic Frameworks Comprising Cobalt Porphyrins for Catalytic CO_2 Reduction in Water. *Science* **2015**, *349*, 1208−1213.
(31) Hemmen, A.; Gross, J. Transferable Anisotropic United-Atom Force Field Based on the Mie Potential for Phase Equilibrium Calculations: n-Alkanes and n-Olefins. *J. Phys. Chem. B* **2015**, *119*, 11695−11707.
(32) Kumar, R. S.; Kumar, S. S.; Kulandainathan, M. A. Highly Selective Electrochemical Reduction of Carbon Dioxide Using Cu Based Metal Organic Framework as an Electrocatalyst. *Electrochem. Commun.* **2012**, *25*, 70−73.
(33) Liang, Z.; Qu, C.; Guo, W.; Zou, R.; Xu, Q. Pristine Metal-Organic Frameworks and Their Composites for Energy Storage and Conversion. *Adv. Mater.* **2018**, *30*, 1702891.
(34) Wang, X.; Chen, Z.; Zhao, X.; Yao, T.; Chen, W.; You, R.; Zhao, C.; Wu, G.; Wang, J.; Huang, W.; Yang, J.; Hong, X.; Wei, S.; Wu, Y.; Li, Y. Regulation of Coordination Number over Single Co Sites: Triggering the Efficient Electroreduction of CO_2. *Angew. Chem., Int. Ed.* **2018**, *57*, 1944−1948.
(35) Kornienko, N.; Zhao, Y.; Kley, C. S.; Zhu, C.; Kim, D.; Lin, S.; Chang, C. J.; Yaghi, O. M.; Yang, P. Metal-Organic Frameworks for Electrocatalytic Reduction of Carbon Dioxide. *J. Am. Chem. Soc.* **2015**, *137*, 14129−14135.
(36) Nam, D.-H.; Bushuyev, O. S.; Li, J.; De Luna, P.; Seifitokaldani, A.; Dinh, C.-T.; García de Arquer, F. P.; Wang, Y.; Liang, Z.; Proppe, A. H.; Tan, C. S.; Todorović, P.; Shekhah, O.; Gabardo, C. M.; Jo, J. W.; Choi, J.; Choi, M.-J.; Baek, S.-W.; Kim, J.; Sinton, D.; Kelley, S. O.; Eddaoudi, M.; Sargent, E. H. Metal-organic Frameworks Mediate Cu Coordination for Selective CO_2 Electroreduction. *J. Am. Chem. Soc.* **2018**, *140*, 11378−11386.
(37) Wang, Y.-R.; Huang, Q.; He, C.-T.; Chen, Y.; Liu, J.; Shen, F.-C.; Lan, Y.-Q. Oriented Electron Transmission in Polyoxometalate-Metalloporphyrin Organic Framework for Highly Selective Electroreduction of CO_2. *Nat. Commun.* **2018**, *9*, 4466.
(38) Xin, Z.; Wang, Y.-R.; Chen, Y.; Li, W.-L.; Dong, L.-Z.; Lan, Y.-Q. Metallocene Implanted Metalloporphyrin Organic Framework for Highly Selective CO_2 Electroreduction. *Nano Energy* **2020**, *67*, 104233.
(39) Dou, S.; Song, J.; Xi, S.; Du, Y.; Wang, J.; Huang, Z. F.; Xu, Z. J.; Wang, X. Boosting Electrochemical CO_2 Reduction on Metal−Organic Frameworks via Ligand Doping. *Angew. Chem., Int. Ed.* **2019**, *58*, 4041−4045.
(40) Wang, B.; Li, W.; Liu, Z.; Duan, Y.; Zhao, B.; Wang, Y.; Liu, J. Incorporating Ni-MOF Structure with Polypyrrole: Enhanced Capacitive Behavior as Electrode Material for Supercapacitor. *RSC Adv.* **2020**, *10*, 12129−12134.
(41) Yuan, X.; Mu, Q.; Xue, S.; Su, Y.; Zhu, Y.; Sun, H.; Deng, Z.; Peng, Y. Polypyrrole Reinforced ZIF-67 With Modulated Facet Exposure and Billion-Fold Electrical Conductivity Enhancement towards Robust Photocatalytic CO_2 Reduction. *J. Energ. Chem.* **2021**, *60*, 202−208.
(42) Gong, Y. N.; Jiao, L.; Qian, Y.; Pan, C. Y.; Zheng, L.; Cai, X.; Liu, B.; Yu, S. H.; Jiang, H. L. Regulating the Coordination Environment of MOF-Templated Single-Atom Nickel Electrocatalysts for Boosting CO_2 Reduction. *Angew. Chem., Int. Ed.* **2020**, *59*, 2705−2709.
(43) Paille, G.; Maria, G.-M.; Catherine, R.-M.; Benedikt, L.-K.; Pierre, M.; Marc, F.; Caroline, M.-D. A Fully Noble Metal-Free Photosystem Based on Cobalt-Polyoxometalates Immobilized in a Porphyrinic Metal-Organic Framework for Water Oxidation. *J. Am. Chem. Soc.* **2018**, *140*, 3613−3618.

https://doi.org/10.1021/acsami.1c15187
ACS Appl. Mater. Interfaces 2021, 13, 54959−54966

(44) Wang, Q.-X.; Zhang, C.-Y. Oriented Synthesis of One-Dimensional Polypyrrole Molecule Chains in a Metal Organic Framework. *Macromol. Rapid Commun.* **2011**, *32*, 1610−1614.
(45) Dhara, B.; Nagarkar, S. S.; Kumar, J.; Kumar, V.; Jha, P. K.; Ghosh, S. K.; Nair, S.; Ballav, N. Increase in Electrical Conductivity of MOF to Billion-Fold upon Filling the Nanochannels with Conducting Polymer. *J. Phys. Chem. Lett.* **2016**, *7*, 2945−2950.
(46) Hoeben, F. J. M.; Jonkheijm, P.; Meijer, E. W.; Schenning, A. P. H. J. About Supramolecular Assemblies of π-Conjugated Systems. *Chem. Rev.* **2005**, *105*, 1491−1546.
(47) Meng, D.-L.; Chen, C.-H.; Huang, J.; Cao, R. Migration-Prevention Strategy to Fabricate Single-Atom Fe Implanted N-Doped Porous Carbons for Efficient Oxygen Reduction. *Research* **2019**, *2019*, 1768595.
(48) Zhang, M. D.; Si, D. H.; Yi, J. D.; Zhao, S. S.; Huang, Y. B.; Cao, R. Conductive Phthalocyanine-Based Covalent Organic Framework for Highly Efficient Electroreduction of Carbon Dioxide. *Small* **2020**, *16*, 2005254.
(49) Uemura, T.; Horike, S.; Kitagawa, K.; Mizuno, M.; Endo, K.; Bracco, S.; Comotti, A.; Sozzani, P.; Nagaoka, M.; Kitagawa, S. Conformation and Molecular Dynamics of Single Polystyrene Chain Confined in Coordination Nanospace. *J. Am. Chem. Soc.* **2008**, *130*, 6781−6788.
(50) Limaye, A. M.; Zeng, J. S.; Manthiram, A. P. W. K. Bayesian Data Analysis Reveals No Preference for Cardinal Tafel Slopes in CO_2 Reduction Electrocatalysis. *Nat. Commun.* **2021**, *12*, 703.

https://doi.org/10.1021/acsami.1c15187
ACS Appl. Mater. Interfaces 2021, 13, 54959−54966